One-dimensional Au on TiO_2

2007 J. Phys.: Condens. Matter 19 082202

(http://iopscience.iop.org/0953-8984/19/8/082202)

IOP FTC

IOP PUBLISHING JOURNAL OF PHYSICS: CONDENSED MATTER

J. Phys.: Condens. Matter **19** (2007) 082202 (8pp) doi:10.1088/0953-8984/19/8/082202

FAST TRACK COMMUNICATION

One-dimensional Au on TiO_2

A Locatelli[1], T Pabisiak[2], A Pavlovska[3], T O Mentes[1], L Aballe[1], A Kiejna[2] and E Bauer[1,3]

[1] Sincrotrone Trieste S.C.p.A., S.S. 14, km 163.5 in Area Science Park, 34012 Basovizza, Trieste, Italy
[2] Institute of Experimental Physics, University of Wrocław, Plac M. Borna 9, PL-50-204 Wrocław, Poland
[3] Department of Physics, Arizona State University, Tempe, AZ 85274-1504, USA

E-mail: ernst.bauer@asu.edu

Received 2 January 2007
Published 6 February 2007
Online at stacks.iop.org/JPhysCM/19/082202

Abstract

One-dimensional Au rows are produced on the $TiO_2(110)$ surface by controlled photon-stimulated desorption followed by Au deposition at 750 K. In the resulting (1×2) structure, O vacancies are replaced by Au atoms, as demonstrated by combined laterally resolved x-ray spectroscopy and micro-LEED (low-energy electron diffraction) measurements. The experimental results are confirmed by first-principles calculations, which indicate strong Au–Ti bonding and a very stable configuration of the Au rows. The calculations determine the detailed atomic structure of the Au rows, with an inter-row spacing of 13 Å and an intra-row Au distance of 2.95 Å.

(Some figures in this article are in colour only in the electronic version)

One-dimensional (1D) metals have long been the subject of scientific interest because of their unique electronic properties [1, 2]. They have been studied in three-dimensional (3D) crystals until the evolution of surface science opened up the possibility of studying them in two-dimensional (2D) systems. One-dimensional metals have been produced by the deposition of sub-monolayer amounts of metals in ultrahigh vacuum on a number of semiconductor surfaces with uniaxial symmetry such as high-index planes or slightly miscut planes with close-packed steps [3]. A recent example is the quasi-one-dimensional system Au on Si(553), which undergoes at least two charge density wave transitions [4]. On Si the Au rows are coupled via the substrate. This coupling is reduced considerably on intrinsic wide-band-gap semiconductors or insulating crystals.

Here we report an experimental and theoretical study of Au on TiO_2, indicating a novel pathway to the creation of one-dimensional structures by Au deposition on ordered bridging oxygen vacancy rows. Au on TiO_2 has been studied extensively in recent years, stimulated by the discovery that the Au, which is inert in macroscopic dimensions, becomes catalytically

active in nanometre-size three-dimensional clusters on reducible oxides [5]. In particular, the oxidation of CO has attracted great attention because of its importance in environmental and renewable energy applications, such as in automotive exhaust catalysts or fuel cell electrodes. This high activity of Au is generally attributed to the strongly modified electronic properties of small clusters. However, recent work indicates that atomically distributed ionic Au also has similar catalytic properties [6]. Finally, two-dimensional Au on ultrathin reduced TiO_2 layers on Mo has also been shown to be highly active [7]. Thus, the effect of dimensionality on reactivity is far from being completely understood for this system.

On a perfect $TiO_2(110)$ surface, Au atoms are very weakly bound, so that they form three-dimensional clusters even at sub-monolayer coverage. Strong bonding occurs only to oxygen vacancy sites [8, 9]. In order to produce one-dimensional structures, these vacancies have to be arranged in a linear fashion. This can be achieved by electron or photon stimulated desorption (ESD or PSD) at sufficiently low temperature so that no significant Ti and O exchange between the surface and volume occurs, but which is high enough (680 K) to allow ordering of the vacancies. ESD and PSD remove the most weakly bound oxygen atoms, which are the bridge-bonded atoms. When the resulting oxygen vacancies reach a sufficiently high density, the repulsive interactions [10] between them lead to ordering, resulting—as will be shown below—in a (1×2) structure. This structure is distinctly different from the (1×2) structure obtained by heating to such high temperatures (>900 K) that considerable oxygen loss occurs from the bulk. In this case, Ti and O diffusion into the bulk leads to a (1×2) surface reconstruction upon cooling [11], for which the so-called added Ti_2O_3 row model (ar(1×2)) is generally accepted now [12]. In the ESD-or PSD-produced (1×2) structure, vacancy equilibration occurs within the surface layer, resulting in a bridge-bonded oxygen missing row (1×2) structure (mr(1×2)). This structure is metastable, because it disorders at slightly higher temperature (720 K). Also, first-principles calculations show that the mr(1×2) structure has a slightly higher total energy than the ar(1×2) structure [13]. Here we concentrate on PSD; the ESD results will be reported elsewhere.

The studies were made in the spectroscopic photo emission and low-energy electron microscope (SPELEEM) at the Nanospectroscopy beamline [14] of the synchrotron radiation facility ELETTRA in Trieste. Micro-spot x-ray photoelectron spectroscopy (μXPS) was used for chemical characterization, and low-energy electron microscopy (LEEM) and LEED for structural characterization, generally after irradiation and at very low electron energy to minimize electron-stimulated desorption of oxygen. The $TiO_2(110)$ crystals, oriented to within less than 0.5° from the [110] direction, were cleaned by alternating sputtering with 600 eV Ar ions and annealing in 3×10^{-6} Torr of oxygen at about 800 K. This treatment produced an excellent (1×1) LEED pattern (figure 1) with a high diffraction peak-to-background ratio and a small half-width of the diffraction peaks, indicating good long-range order with few defects.

The experiments are performed as follows. The photon beam ($h\nu = 170$ eV), focused into a band 5 μm wide and 20 μm long (FWHM), is used to produce regions with different oxygen vacancy densities by irradiation with a flux density of about 1.5×10^{11} photons s^{-1} μm^{-2} for different times at about 750 K. With increasing irradiation doses, the initial (1×1) LEED pattern evolves into a (1×2) pattern, indicating vacancy ordering, until an optimum (1×2) pattern ('(1×2)-V') is obtained (figure 1). At higher doses the (1×2)-V pattern deteriorates. Irradiation at higher temperatures produces poorer order. The vacancy concentration is calibrated by assuming that the optimum (1×2) structure occurs at a vacancy coverage of 0.5 monolayer (ML). The $I(V)$ curves at this coverage look distinctly different from those of the ar(1×2) structure. After the preparation of regions with different vacancy densities, Au is deposited at various coverages up to 2 ML at the same temperature. The Au coverage is calibrated in an independent experiment by high-temperature deposition on a

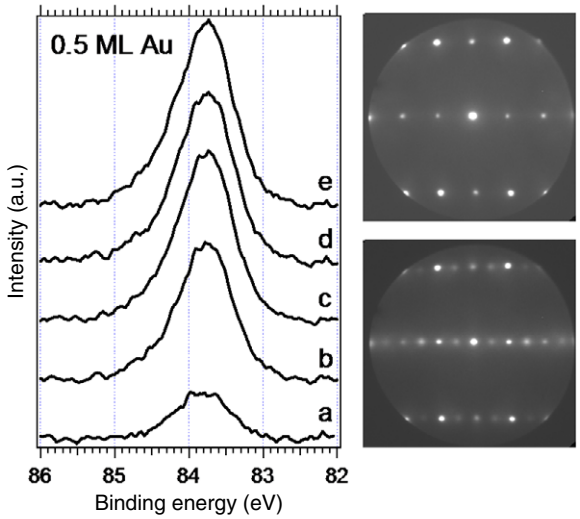

Figure 1. Left: Au $4f_{7/2}$ spectra as a function of the irradiation dose for 0.5 ML Au coverage—(a) unirradiated surface; ((b)–(e)) increasing irradiation doses, as indicted by open circles in figure 2. Right: LEED patterns of the (1×1) and the (1×2) structures.

W(110) surface. On the TiO_2 surface the adsorbed Au atoms form 3D clusters in regions with single or no vacancies, leaving the LEED pattern unchanged. Au diffusion to vacancy rows converts these rows into Au rows. The resulting (1×2)-Au LEED pattern is, in general, only slightly different from that of the Au-free surface. In particular, neither the background, which is a measure of disorder, nor the peak intensities change upon the deposition of 0.5 ML of Au.

The Au distribution in the unirradiated and in the irradiated regions is determined by μXPS of the Au 4f spectrum from an area of about 3 μm^2. The photon energy is chosen to minimize the inelastic mean free path of photoelectrons in Au (about 3 Å at 95 eV) [15]. This ensures optimum discrimination between 3D clusters and 1D and 2D distributions because of the strong photoelectron screening in 3D clusters. Figure 1 shows typical Au $4f_{7/2}$ spectra of a 0.5 ML thick Au film from regions with different irradiation doses, i.e. with different vacancy densities. The Au 4f peak position is independent of irradiation dose, even at the highest dose at which significantly more than 0.5 ML of bridging oxygen atoms have been removed.

At all Au coverages studied, the Au 4f signal increases rapidly from zero dose value to the first dose and then slowly to the last dose, as shown in the lower part of figure 2. For comparison, the top part of this figure shows the intensity of the LEED (0, 1/2) beam. The Au 4f signal changes slope coincident with the maximum of the (0, 1/2)-order LEED intensity, when the (1×2) pattern is most perfect ('(1×2)-V'), i.e. at a vacancy coverage of 0.5 ML. The Au 4f signal at zero irradiation dose is from three-dimensional clusters which very likely nucleate at randomly distributed oxygen vacancies. The drastic intensity difference between unirradiated regions and the region with 0.5 ML vacancies is a clear indication of a growth mode change from three- to either two- or one-dimensional, while the strong preference of Au to adsorb on O vacancies, which form rows, clearly favours a one-dimensional scenario. The slower change of the Au signal after the initial strong rise corresponds to the filling of vacancies in excess of 0.5 ML by Au atoms diffusing into the irradiated regions from the unirradiated surrounding, where the Au atoms are bound much more weakly. The scatter of the data points is due to the shape of the photon beam, which has a Gaussian intensity profile. This causes a corresponding irradiation distribution, resulting in an inhomogeneous vacancy distribution.

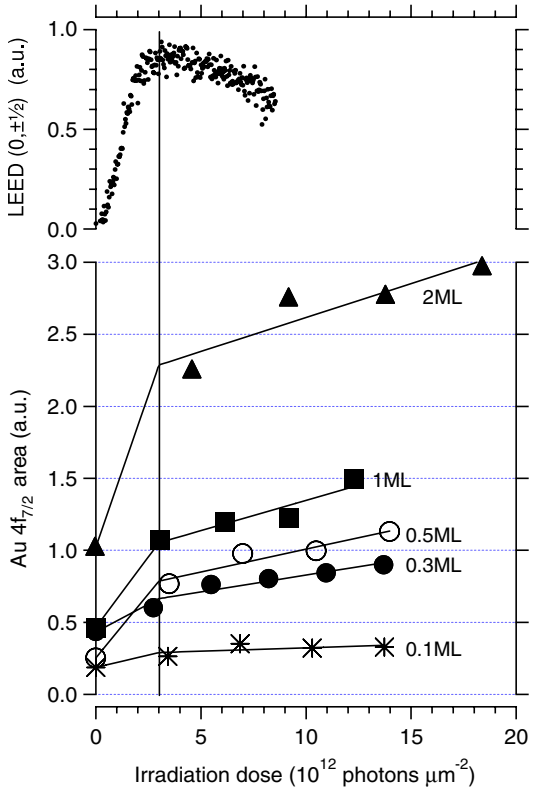

Figure 2. Bottom: area of Au $4f_{7/2}$ core level emission peak as a function of the irradiation dose for experiments with different Au coverage, as indicated on the graph. Top: corresponding intensity of the LEED (0, 1/2) order spot.

Summarizing the experimental results, the μXPS results show that in regions with high vacancy concentration the Au atoms do not form 3D clusters but are 2D distributed. The LEED results show that the distribution is not random but that the Au atoms form 1D rows in the vacancy rows, with an intra-row spacing of 2.95 Å and an inter-row spacing of 13 Å. The increase of the Au 4f signal with increasing Au coverage suggests that not only one Au row but up to three or more rows can be adsorbed in the oxygen vacancy rows.

In order to obtain a more detailed picture of the arrangement of the Au atoms, in particular of the dimer and trimer rows, we have resorted to first-principles calculations, which not only give the detailed structure but also the bonding. Both the missing row and the added row model with monomer, dimer and trimer Au rows were considered. The calculations apply density-functional theory, with plane-wave basis ($E_{\rm cut} = 400$ eV) and the projector augmented-wave potentials [16], as implemented in the VASP code [17]. The exchange–correlation energy accounts for spin polarization within the generalized gradient approximation [18]. The rutile $TiO_2(110)$ surfaces are modelled with a (1×2) surface unit cell on symmetric slabs of five TiO_2 layers, separated by 16 Å of vacuum. Full relaxation of the structure was applied in each case (forces on atoms <0.02 eV Å^{-1}). Other details are similar to those given in [19]. Both the missing row (mr) and the added row (ar) models were considered. We analyse the adsorption binding energy, $E^{\rm ad} = -(E^{\rm Au/sub} - E^{\rm sub} - 2NE^{\rm Au})/2N$. Here $E^{\rm Au/sub}$ is the total energy of the slab covered with N Au atoms, $E^{\rm sub}$ is that of the Au-free surface slab, and $E^{\rm Au}$ is the energy of an isolated Au atom.

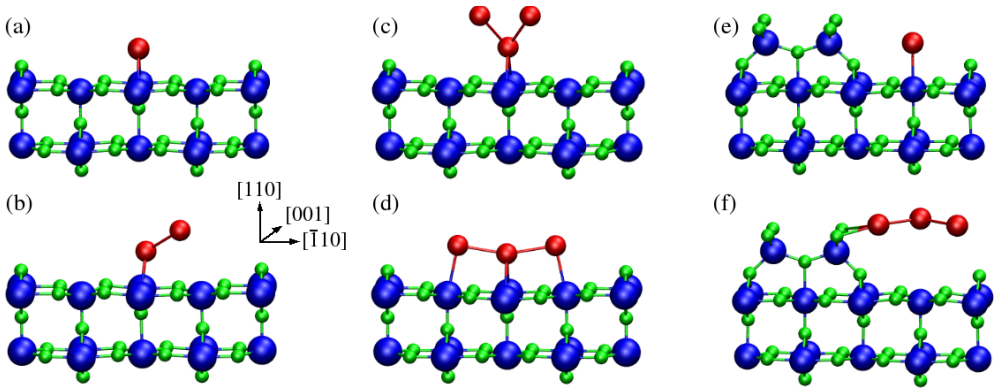

Figure 3. Atomic configurations of $TiO_2(110)$. Large, intermediate-size and small balls indicate Ti, Au and O atoms, respectively. (a)–(d) Side views of the mr(1×2) surface unit cell showing final adsorption sites for monomer (a), dimer (b) and trimer ((c), (d)) Au rows with the additional Au atoms originally bridging Ti(5c) atoms (c), or above Ti(5c) atoms (d). (e) Monomer and (f) trimer Au rows on the ar(1×2) surface.

Table 1. Adsorption energy per atom, E^{ad}, the Au–Au bond length, and the bond length between Au and the surface Ti(6c) or Ti(5c), for Au rows adsorbed on the mr(1×2) and on the ar$(1 \times 2)TiO_2(110)$ surfaces, respectively. The labels (a)–(f) refer to figure 3.

Structure		E_{ad} (eV)	d_{Au-Ti} (Å)	d_{Au-Au} (Å)
Monomer row	mr (a)	2.83	2.67	—
	ar (e)	1.56	2.68	—
Dimer row	mr (b)	2.51	2.73	2.78
	ar	2.06	3.19	2.69
Trimer row	mr (c)	2.42	2.78	2.85
	mr (d)	2.25	2.79	2.74
	ar (f)	2.25	4.78	2.70

The formation of defects, reconstruction of the surface, or Au adsorption lead to shifts in atomic positions. In the mr structure, the displacements in the [110] direction (with respect to the average z-position of the central Ti layer) differ significantly from those for stoichiometric slabs. The lack of bridging oxygen (O^{bri}) causes major outwards relaxations of the in-plane oxygens (0.28 and 0.44 Å) and of the six-fold-coordinated Ti(6c) atoms (0.23 Å). The Ti atoms underneath the vacancy row shift 0.15 Å inwards. However, via Au adsorption the distances are much recovered, so that the interlayer spacings are only altered a little ($<1\%$) compared to the bulk.

Monomer Au rows. The monomer Au row binds strongly to the mr but much weaker to the ar surface (see table 1), though the Au–Ti bond lengths for the mr and ar surfaces are quite close. The corresponding work function increases compared to the clean surface are 0.32 and 0.14 eV. Figure 4 displays iso-surfaces of the electron density difference due to Au bonding on the mr surface. They are calculated as the difference in electron charge densities of the complete adsorption system and that of the mr(1×2) $TiO_2(110)$ slab, and the free Au atoms at the positions of the relaxed Au/TiO_2. Judging by the electron charge gain for a single O^{bri} row replaced by an Au row, the bonding of Au is mainly to the Ti atoms below, and to the neighbouring Au atoms.

Dimer Au rows. Dimer Au rows on the mr(1×2) surface consist of stable, tilted dimers (figure 3(b)), with 0.3 eV/atom weaker binding than in the monomer Au row. Stable dimer

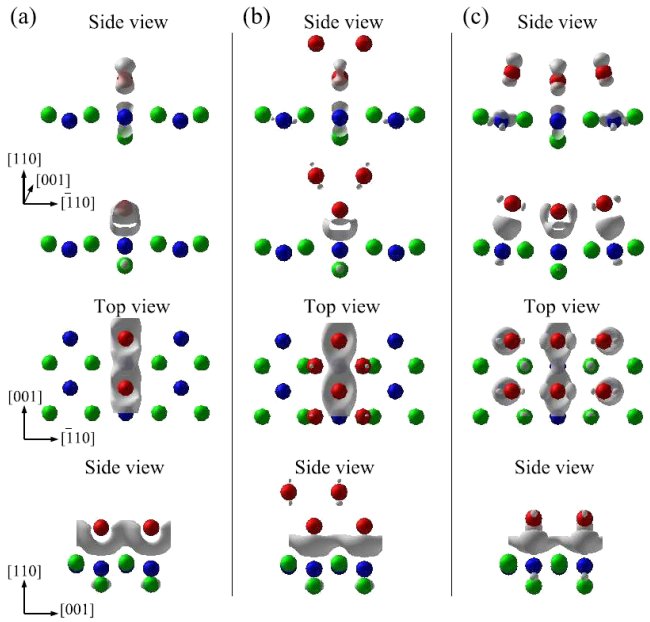

Figure 4. Electron density changes upon Au adsorption on the mr(1 × 2) surface. Iso-charge contours in all graphs correspond to ±0.03 electron Å^{-3}. (a) Monomer Au row (figure 3(a)); (b) trimer Au row (figure 3(c)); (c) trimer Au row (figure 3(d)). First row contours display the charge loss, whereas the remaining ones display the charge gain. Black (blue/green) balls represent Ti and Au, grey (red) balls represent oxygen atoms.

rows are also formed on the ar(1 × 2) surface (not shown), but their binding is weaker than on the mr(1 × 2) surface. Bonding of Au is mainly to the Ti atoms below, and to the neighbouring Au atoms.

Trimer Au rows. The additional Au atoms placed between the atoms of Ti(5c) rows (figure 3(c)) do not adsorb over these sites but displace ≈2 Å towards the central Au atom, and shift 4.4 Å away from the surface to form a three-dimensional Au row, together with the central Au atom. On the mr surface the binding energy/atom (see table 1) is lower than that in the monomer and dimer row, while on the ar surface the reverse is true. The Au–Ti bond length of the central Au atom increases only slightly (≈0.1 Å) on the mr surface but strongly (≈2.1 Å) on the ar surface compared to the monomer row. However, the displacements of the surface layers are almost unaltered. If the additional Au atoms are initially placed over the Ti(5c) atoms (figure 3(d)), they shift almost three times (≈0.6 Å) less towards the central Au row. Their positions above the surface are only about 0.5 Å higher than that of the central row Au atoms, but they are more weakly bound by 0.17 eV (table 1) than in the configuration of figure 3(c). The buckling of the surface layer is significantly reduced, compared to the previous case.

The changes in the electron density distribution in the three systems show (figure 4) that the adsorption of additional Au rows between Ti(5c) atoms (figure 3(c)) and over the Ti(5c) atoms (figure 3(d)) is characterized by a distinctly different bonding. In the first case, the additional Au atoms are rather weakly bound to the Au atoms of the central row. The binding of the central Au to the surface is also weakened, judging by the reduced binding electron charge and the increased distance of the Au from the surface (2.39 Å for the bottom Au in a triple row, compared to 2.29 Å for Au in the single row). Neither an intra-row bonding nor bonding

Table 2. The amount of electron charge transfer of different electrons (treated as valence electrons in the PAW potentials applied) in a sphere of radius $R_{Au} = 1.40$ Å, drawn around a Au atom, as given by the difference between an isolated Au atom and one bound to the surface. For labelling, see figure 3.

Structure	Atom	s	p	d	Tot
Single	Au(a)	0.259	0.087	−0.215	0.132
Triple	Au(c) bottom	0.133	0.088	−0.136	0.084
	Top	0.017	−0.006	0.008	0.019
Triple	Au(d) bottom	0.140	0.058	−0.101	0.197
	Top	0.093	0.029	−0.063	0.058

of the additional Au rows to surface atoms can be seen. In the second case (figure 3(d)), the accumulated electron charge shows that the bonding of the central (bottom) Au to the surface is further weakened compared to the former case, at the expense of the binding of additional Au rows to the surface. The Au atoms in the additional rows bond predominantly to the surface Ti(5c) atoms, while those of the central row bond mostly along the Au row. The charge redistribution in the Au atoms caused by the adsorption bond is also described by the difference in charge enclosed in spheres drawn around the free and adsorbed Au atoms. The calculated charge transfer (table 2) in the Au atoms clearly shows that the bonding between Au and surface atoms is determined by the electron transfer from the localized d-states to the more extended s-states. The charge density distribution of figure 4 suggests metallic behaviour of the Au rows, which is confirmed by the increase in the density of occupied states around the Fermi edge (not shown).

Summarizing the experimental and theoretical results, Au forms on the reduced $TiO_2(110)(1 \times 2)$ surface strongly adsorbed one-dimensional rows which consist of one to up to three or more Au atoms per row unit cell, depending on Au coverage. The strong bonding of Au atoms to oxygen vacancies ensures that initially monomer rows form. The higher binding energy per atom in the dimer rows than in the trimer rows suggests that dimer rows form before trimer rows. Intra-chain and inter-chain spacings are determined by the substrate periodicity. The LEED observations indicate that the surface has the missing row structure. The bonding of the single Au row to the added row structure is much weaker than to the missing row structure or to three-dimensional Au clusters, which supports the missing row model. The bonding to the substrate is predominantly covalent, with little charge transfer to the Au atoms. The large inter-chain distance (13 Å) on the more or less insulating substrate makes this system ideal for studies of one-dimensional phenomena.

The authors wish to thank M Kiskinova for critical comments. AP and EB thank the the US National Science Foundation for support under project number 0315412.

References

[1] Roth S and Carroll D 2004 *One-dimensional Metals: Conjugated Polymers, Organic Crystals, Carbon Nanotubes* (Weinheim: Wiley–VCH)
[2] Giamarchi T 2004 *Quantum Physics in One Dimension* (Oxford: Oxford University Press)
[3] Himpsel F *et al* 2001 *Solid State Commun.* **117** 149
Himpsel F *et al* 2001 *J. Phys.: Condens. Matter* **13** 11097
Himpsel F *et al* 2004 *J. Phys. Chem.* B **108** 14484
[4] Snijders P C, Rogge S and Weitering H H 2006 *Phys. Rev. Lett.* **96** 076801
[5] Haruta M 2003 *Chem. Record* **3** 75

[6] Fu Q, Saltsburg H and Flytzani-Stephanopulos M 2003 *Science* **301** 953
[7] Chen M S and Goodman D W 2004 *Science* **306** 252
[8] Vijay A, Mills G and Metiu H 2003 *J. Chem. Phys.* **118** 6536
[9] Wang Y and Hwang G 2003 *Surf. Sci.* **542** 72
[10] Rasmussen M D, Molina L M and Hammer B 2004 *J. Chem. Phys.* **120** 988
[11] McCarty K and Bartelt N 2003 *Surf. Sci.* **527** L203
[12] Fukui K *et al* 2003 *Phys. Chem. Chem. Phys.* **5** 5349
[13] Ng K-O and Vanderbilt D 1997 *Phys. Rev.* B **56** 10544
[14] Locatelli A *et al* 2003 *J. Physique* IV **104** 99
Locatelli A *et al* 2006 *Surf. Interface Anal.* **38** 1554
[15] Ding J and Shimizu R 1996 *Scanning* **18** 92
[16] Kresse G and Joubert D 1999 *Phys. Rev.* B **59** 1758
[17] Kresse G and Furthmuller J 1996 *Phys. Rev.* B **54** 11169
Kresse G and Furthmuller J 1996 *Comput. Mater. Sci.* **6** 15
[18] Perdew J P, Burke K and Ernzerhof M 1996 *Phys. Rev. Lett.* **77** 3865
[19] Kiejna A, Pabisiak T and Gao S 2006 *J. Phys.: Condens. Matter* **18** 4207